Journal of Sound and Vibration (1998) **218**(1), 81–101
Article No. sv981777

AN IMPROVED MODEL OF A PNEUMATIC VIBRATION ISOLATOR: THEORY AND EXPERIMENT

C. Erin and B. Wilson
Department of MIME, Northeastern University, Boston, MA, U.S.A.
and
J. Zapfe
Acentech, Inc., Cambridge, MA, U.S.A.

(*Received* 18 *December* 1997, *and in final form* 2 *June* 1998)

The design of an active controller for a vibration isolation table employing pneumatic vibration isolators requires an accurate mathematical model of the isolator. An experimental investigation of the validity of available models has been performed and indicates significant errors between predicted and observed behavior. An analysis of the model and the data suggested that a previously ignored component of the isolator, the diaphragm, plays a significant role in isolator response. This paper develops the modifications to the standard isolator model that incorporate the effects of the diaphragm. When the diaphragm is included in the isolator model, the modified model predicts time-domain and frequency-domain behavior quite closely. We conclude that the modified model of the pneumatic isolator improves markedly the accuracy of the predictions provided by the model.

1. INTRODUCTION

Vibration isolation tables, which are intended to isolate a payload from floor (base) motion, find application in optical experiments, semiconductor manufacturing and precise measurement. The tables are also intended to provide some degree of force disturbance rejection, where the force can originate from the payload itself or from an external source [1]. A stiff table top, stiff legs and relatively flexible vibration isolators form the key components of an isolation table. Some designs use legs with air-filled chambers, an elastomeric diaphragm and a piston [2, 3]. The chambers are pressurized so that the piston can support a range of loads. This configuration, the pneumatic vibration isolator, is shown in Figure 1. Other designs use a pressurized fiber reinforced torus to support a payload. This configuration will likely have different characteristics than the air-filled chambers and diaphragm considered in this paper. The configuration that will be our focus is illustrated in Figure 1.

0022–460X/98/460081 + 21 $30.00/0

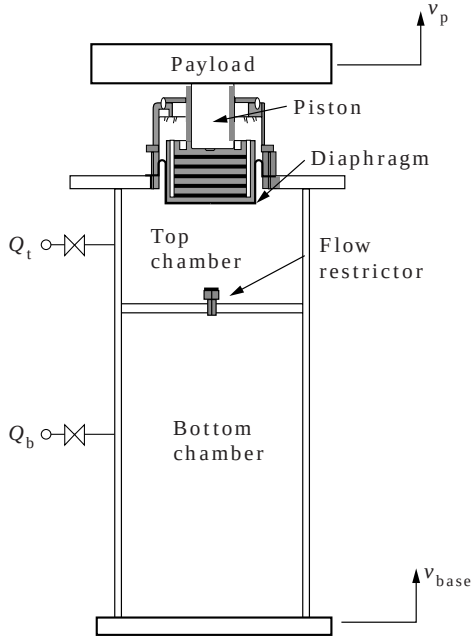

Figure 1. Pneumatic vibration isolator.

An effort to design an active levelling system created the need for an accurate mathematical model of the pneumatic vibration isolator. Existing models of pneumatic vibration isolators are based on non-linear models for pneumatic cylinders. These non-linear models, after some simplifying assumptions, enable the development of linear models around a nominal operating point. The accuracy of the models, both non-linear and linearized, is contingent on the validity of the assumptions used in developing the models. Previous studies on pneumatic vibration isolators [4, 5] assumed, without validation, that these models closely predict system behavior. However, experimental results provided here indicate rather large discrepancies between predicted and observed behavior. A hitherto ignored mechanism, the isolator diaphragm, has been found to have a significant effect on isolator performance. When this mechanism is added to the model, predicted and observed behavior correspond quite closely.

1.1. BACKGROUND

Models of pneumatic vibration isolators are based on non-linear models of pneumatic cylinders. These pneumatic cylinders are used in servo applications. Models of pneumatic cylinders were first proposed by Shearer [6, 7]. These models include the enthalpy equations for the pneumatic chambers, a flow equation for the restrictor connecting the chambers, and the equation of motion for the piston supporting the payload. Shearer's models are non-linear, with the basic non-linearities resulting from orifice flow in the flow restrictor and gas compressibility in the chambers. In these models, chamber equations have been

derived for two extreme cases: one that assumes adiabatic behavior and the other that assumes isothermal behavior.

Linear models derived from the non-linear precursors facilitate the analysis of pneumatic vibration isolators. Harris and Crede [8] propose the first linear model of the pneumatic vibration isolator. The linearity of this model is obtained by assuming small payload displacements and by replacing non-linear orifice flow with incompressible-fully-developed-laminar flow through the flow restrictor. Analysis performed on this new model clarifies the effect of the flow restrictor on system behavior [8]. These analyses suggest that large payload displacement amplitudes render large pressure gradients between the two chambers, which cause non-linear turbulent flow through the flow restrictor. The analysis also indicates that the payload's vibration frequency affects the flow through the flow restrictor. Hence, the pneumatic vibration isolator provides non-linear damping due to the non-linearities associated with the flow restrictor.

A simpler linear model of the pneumatic vibration isolator, using three parameters to represent the system, is derived by DeBra [4]. These three parameters include the isolator natural frequency, the chamber volume ratios and a frequency factor, which is a function of the isolator natural frequency. This model is used for designing pneumatic vibration isolators providing linear damping characteristics. Analysis suggests that if the flow restrictor is designed to operate on the laminar flow region, the isolator will provide linear damping at all payload displacement amplitudes [4]. Further endeavors employ this model to simulate whole table response for moving payloads [5].

1.2. OVERVIEW OF THE PAPER

The outline of this paper is as follows. Section 2 reviews the existing models of pneumatic vibration isolators and develops a standard linear model. The predictions provided by the standard model are compared with measured data in section 3, where a large discrepancy between predicted and observed behavior is noted. This discrepancy requires a modification to the standard model, which is described and experimentally verified in section 4. The paper closes with some conclusions in section 5.

2. MATHEMATICAL MODEL OF A TWO-CHAMBER ISOLATOR

Mathematical models of the pneumatic vibration isolator in Figure 1 consist of thermodynamic equations for the top and bottom chambers and the equation of motion for the piston supporting the payload. The nature of the flow through the restrictor and the compressibility of air render these models non-linear. This non-linear characteristic complicates the analysis of the system. However, the linearization of the model around a nominal operating point eliminates these non-linearities. In the sequel, the non-linear system equations will be presented first. These equations will then be linearized via a Taylor series expansion. Finally, we will derive the transfer functions for base motion input and force disturbance input, which will be used to verify the model.

2.1. NON-LINEAR MODEL

Pneumatic vibration isolators are cylinders designed for vibration control. Therefore, non-linear mathematical models for pneumatic cylinders [6, 7] form the basis of the models for pneumatic vibration isolators. Non-linear models of the pneumatic vibration isolator derived from these models consist of the enthalpy equations for the top and bottom chambers and the equation of motion for the piston, derived using Newton's second law. The pneumatic vibration isolator is a complicated system; the following assumptions simplify its analysis:

Ideal gas law

The ideal gas law can be used for a system when the operating pressures and temperatures are not close to the system's critical pressures and temperatures. As the typical pressures and temperatures in this system meet this condition, the ideal gas law will be utilized throughout the analysis.

Adiabatic process

Adiabatic processes are fast processes in which the system does not have sufficient time to exchange heat with the surroundings. Pneumatic vibration isolators, with settling times on the order of seconds, are considered fast systems. Therefore, an adiabatic process assumption will be employed.

Gas dynamics

The size of an isolator chamber and the speed of sound determine the time it takes for the gas to reach a uniform state. Since typical chambers have dimensions on the order of 10 cm and the speed of sound in air is approximately 343 m/s, the time it takes for the gas to reach a uniform state is negligibly small. Therefore the gas is assumed to mix instantaneously (i.e., is continuously uniform) in the top and bottom chambers, so that a single pressure and temperature describe the state of the fluid in each chamber.

Direction of motion

Fluid dynamic effects within the pneumatic mount are assumed to only depend on the vertical displacement of the payload; hence the mount dynamics are considered in this direction only.

Constant temperature

For the passive system, the temperature deviation depends on the magnitude of the payload displacement and the amount of mass exchange between the chambers. Since typical payload displacements are on the order of 1–100 μm and the amount of mass exchange between the chambers in a pneumatic isolator is minimal, temperatures in the chambers are assumed to be equal and constant.

Fully developed flow

The flow through the restrictor is fully developed because the flow restrictor has a length-to-diameter ratio >10 [9]. Further, if the Reynolds number (Re) is

<2000, the flow is laminar and a linear relation exists between the flow rate and the pressure gradient [10, 11].

Diaphragm dynamics

The piston and the payload are assumed to be supported only by the gas in the top chamber, and the effect of the diaphragm is ignored. However, in the course of subsequent analysis, this assumption is seen to be invalid; it will be dropped in section 4.

The non-linear model is derived first by considering the energy processes in the top chamber. The rate at which energy leaves the top chamber is found by multiplying the total energy content per unit weight of gas, $C_p T$, by the weight rate of flow, $\dot{W}_t$. The total energy content, H, consists of the internal energy of the gas at a particular temperature, U, and the energy gained or lost by the gas as a result of its compression or expansion, E. This is expressed as the rate of change of enthalpy:

$$\dot{H} = \dot{U} + \dot{E} = \dot{W}_t C_p T. \tag{1}$$

The rate of change of internal energy of the gas in the cylinder and the rate of change of energy in the gas as a result of work done on or by the gas equal

$$\dot{U} = \dot{W}_t C_v T = \frac{gC_v}{R}\frac{d}{dt}(P_t V_t), \qquad \dot{E} = gP_t \dot{V}_t. \tag{2a, b}$$

After substituting equations (2) into equation (1), and rearranging using the expression $1/R = 1/C_p + 1/(nR)$, the equation for the top chamber can be written as

$$\dot{m}_t = \frac{1}{RT}\left[\frac{V_t}{n}\dot{P}_t + P_t \dot{V}_t\right]. \tag{3}$$

For the bottom chamber, equation (3) can be used with a slight modification. Since there is no volume change associated with the bottom chamber (i.e., $\dot{V}_b = 0$), the equation for the bottom chamber can be written as

$$\dot{m}_b = \frac{1}{RT}\frac{V_b}{n}\dot{P}_b. \tag{4}$$

Equations (3) and (4) constitute a model for the top and bottom chambers. The mass flow rates into the top and bottom chambers and the volume of the top chamber, $\dot{m}_t$, $\dot{m}_b$ and V_t, will be respectively defined as

$$\dot{m}_t = -\dot{m}_{tb} + \rho Q_t, \qquad \dot{m}_b = \dot{m}_{tb} + \rho Q_b, \tag{5a, b}$$

$$V_t = A_p x_p + V_{t_0} - A_p x_{base}. \tag{5c}$$

The mass flow rate through the flow restrictor connecting the top and bottom chambers in equations (5), $\dot{m}_{tb}$, is defined as

$$\dot{m}_{tb} = \rho C_r (P_t - P_b), \qquad C_r = \frac{\pi d^4}{128\,\mu l}, \tag{6a, b}$$

which is valid when $l/d > 10$ and $\mathrm{Re} < 2000$. We will calculate the Reynolds number in the sequel. Finally, the equation of motion for the piston is obtained using Newton's second law,

$$m_p \dot{v}_p = F_d + A_p(P_t - P_{atm}) - m_p g. \tag{7}$$

Equations (3)–(7) characterize the pneumatic vibration isolator. The inputs to the system are the volume flow rates of gas through the valves, Q_t and Q_b, the base displacement, x_{base}, and the disturbance force acting on the payload, F_d. The non-linearities in the system are evident in equations (3) and (6a). Non-linearity due to gas compressibility occurs in equation (3), where the gas density, $\rho = P_t/RT$, is not constant. Non-linearity due to the flow through the flow restrictor occurs in equation (6a), where the gas density, ρ, is again changing with pressure.

2.2. LINEARIZED MODEL

Linear models [4, 8] are more efficient for analysis when compared to non-linear ones, because the coupling mechanism between the system inputs, the state variables and the outputs is easier to understand. Furthermore, simulation and analysis tools exist for linear models, which makes linear models more convenient. Therefore, linear models have been used to represent the pneumatic vibration isolator. Before introducing these linear models, we will discuss their suitability.

A system can be represented by a linear model if it operates around a nominal operating point with small displacements. In their normal operating mode, pneumatic vibration isolators isolate a payload from base motion. Typical base motion amplitudes acquired are on the order of 10 μm; consequent payload displacements are smaller than this value. Therefore, in this mode the system operates around a nominal point with small displacements. In contrast to base motion input, large amplitude disturbance forces produce large displacements on the order of millimeters. However, for forces on the order of 50 N, the payload displacements are sufficiently small for linearization. Small payload displacements result in pressure differentials that are small compared to the nominal operating pressures. Hence, through the ideal gas law, the density of the gas in the chambers will be assumed to be constant. Note that the proposed range of forces for linearization is appropriate for the specific hardware discussed in this paper. Significant changes in model parameters or applied forces would require a re-examination of the linearity assumption.

Based on the premises in the previous paragraph, a linear model for the isolator is constructed. The linear model is derived by performing a Taylor series expansion of the non-linear model around the nominal operating point, which corresponds to the static equilibrium position of the payload. The state variables in this model are the differential pressures of the top and bottom chambers, δP_t and δP_b, and the differential displacement and velocity of the payload, δx_p and δv_p. The nominal state for the system corresponds to the constant pressures in chambers supporting the payload and the static equilibrium position of the payload. The linearization process involves the Taylor series expansion of equations (3), (4) and (7) around the nominal operating point. First-order Taylor series will be used in this

linearization. First the substitutions (6a)→(5a)→(3) and (6a)→(5b)→(4) are made. Then equations (3), (4) and (7) are solved for $\dot{P}_t$, $\dot{P}_b$ and v_p respectively. The Taylor series expansion of these three equations yields the following linear model for the pneumatic vibration isolator:

$$\delta\dot{P}_t = -\frac{nRT\rho C_r}{V_{t_0}}\,\delta P_t + \frac{nRT\rho C_r}{V_{t_0}}\,\delta P_b - \frac{nA_pP_0}{V_{t_0}}\,\delta v_p + \frac{nA_pP_0}{V_{t_0}}\,\delta v_{base} + \frac{nRT\rho}{V_{t_0}}\,Q_t, \tag{8a}$$

$$\delta\dot{P}_b = -\frac{nRT\rho C_r}{V_b}\,\delta P_b + \frac{nRT\rho C_r}{V_b}\,\delta P_t + \frac{nRT\rho}{V_b}\,Q_b, \tag{8b}$$

$$\delta\dot{v}_p = \frac{A_p}{m_p}\,\delta P_t + \frac{1}{m_p}\,F_d. \tag{8c}$$

The differential payload displacement, δx_p, vanishes in equation (8), which reduces the number of state variables to three. The delta sign in the state variables represents the deviation of those states from the nominal operating point (i.e., $\delta P_i = P_i - P_0$). Since the nominal operating pressures for the top and the bottom chambers are equal, a single pressure, P_0, will be used to represent this value. The valve flow rates, Q_t and Q_b, are zero for the passive system.

2.3. TRANSFER FUNCTIONS

Transfer functions facilitate the analysis of the response of a system for specific inputs, e.g., a frequency response plot is readily obtained. In a passive pneumatic vibration isolator, base motion and disturbance force are the two inputs of interest. The isolator response for these two inputs is depicted by two different sets of data: transmissibility and force disturbance response. Transmissibility, the ratio of payload displacement to base displacement, characterizes the system response to base motion input. Force disturbance response is the ratio of payload displacement to the disturbance force applied to the payload. After transforming the linear model (8) into the Laplace domain, the following transfer functions result:

$$\frac{x_p(s)}{x_{base}(s)} = \frac{\dfrac{nP_0A_p^2}{V_{t_0}}\left(s + \dfrac{nP_0C_r}{V_b}\right)}{m_ps^3 + \dfrac{m_pnP_0C_rV_{t_0} + V_b}{(V_{t_0}V_b)}\,s^2 + \dfrac{nP_0A_p^2}{V_{t_0}}\,s + \dfrac{n^2P_0^2C_rA_p^2}{V_{t_0}V_b}}, \tag{9}$$

$$\frac{x_p(s)}{F_d(s)} = \frac{s + \dfrac{nP_0C_rV_{t_0} + V_b}{(V_{t_0}V_b)}}{m_ps^3 + \dfrac{m_pnP_0C_rV_{t_0} + V_b}{(V_{t_0}V_b)}\,s^2 + \dfrac{nP_0A_p^2}{V_{t_0}}\,s + \dfrac{n^2P_0^2C_rA_p^2}{V_{t_0}V_b}}. \tag{10}$$

These transfer functions describe the complicated coupling mechanism in pneumatic vibration isolators. The transfer functions of the pneumatic vibration isolator (9) and (10) have a third order denominator.

TABLE 1
Parameter values used in simulations

Symbol	Description	Value
d	Flow restrictor diameter	6·10E − 04 m
g	Gravitational acceleration	9·81 m/s^2
l	Flow restrictor length	7·27E − 03 m
m_p	Payload mass	110 kg
n	Polytropic exponent	1·4
A_p	Effective piston area	1·85E − 03 m^2
C_r	Flow restriction constant	2·55E − 08 m^3/(s · Pa)
P_{atm}	Atmospheric pressure	101 325 Pa
R	Universal gas constant	286·9 Pa·m^3/(kg · K)
T	Temperature	298 K
V_b	Bottom chamber volume	4·18E − 04 m^3
V_{to}	Top chamber volume	7·32E − 05 m^3
μ	Air viscosity	1·824E − 05 Pa · s

3. MODEL VERIFICATION

Closed-loop controller design requires an accurate model of the *plant* dynamics. To check the suitability of the isolator model in this context, we will evaluate experimentally the performance of this model.

3.1. EXPERIMENTAL APPARATUS

Successful application of the models presented requires that they predict the actual system response accurately. To check the accuracy of these models, we will evaluate their responses against experimental data. Transmissibility and force disturbance response will be used in the validification. For transmissibility, typical base motion involves very small displacements, resulting in small payload displacements. Therefore, the system response is linear for base motion inputs. In contrast, force disturbance response involves relatively large inputs and large payload displacements, which result in a non-linear behavior.

The experimental apparatus used to measure transmissibility and force disturbance response employs a pneumatic mount (the isolator), accelerometers, a Fourier analyzer and a PC. Figure 1 shows the mount used in testing. This mount is located on a flat base. The chambers of the mount are pressurized with air to support a payload of 110 kg. Accelerometers located on the payload and the base of the isolator sense the payload and base motion. These sensed accelerations, after signal conditioning with an amplifier, are fed to the Fourier analyzer. The analyzer, connected to a PC, performs the arithmetic operations on the signals and provides the experimental transmissibility and force disturbance response data. The transmissibility tests are performed by sensing the payload response for base motion input. The force disturbance tests involve monitoring of the payload response for known mass removals from the payload.

We will examine transmissibility and force disturbance response for two distinct mounts. The first mount involves a dual-chamber pneumatic vibration isolator

with the dimensions stated in Table 1. The second mount is identical to the first, except that the flow restrictor between the chambers is plugged. This seals the lower chamber and leads to a single-chamber isolation mount. As the single-chamber mount has a much smaller volume than the two chamber mount, it will have less compliance and a correspondingly higher natural frequency. The models developed in section 2 assume that the only element providing damping to the pneumatic vibration isolator is the flow restrictor. When the restrictor is plugged, as in the case of the single-chamber mount, the isolator model has no damping.

3.2. PREDICTED AND OBSERVED RESPONSES

The apparatus described in the previous section provides the means to measure behavior that will be compared with theoretical responses. We will first compare the measured and theoretical transmissibilities for the dual-chamber system, which are shown in Figure 2. We see a rather large discrepancy between the theoretical and experimental transmissibility curves. The theoretical resonant frequency of the system is 1·24 Hz; whereas the measured data indicates a 1·85 Hz resonant frequency. The theoretical model underestimates the resonant frequency by 33%. Note in Figure 2 the presence of the second peak in the experimental data. A rocking mode of the apparatus causes this second resonance. The isolator model does not include this mode. A perfectly centered payload would eliminate the rocking mode, but such centering is difficult to achieve in practice. As this mode has little effect near the fundamental frequency of the isolator and the mode is an artifact of the apparatus, we will ignore this mode in subsequent analysis.

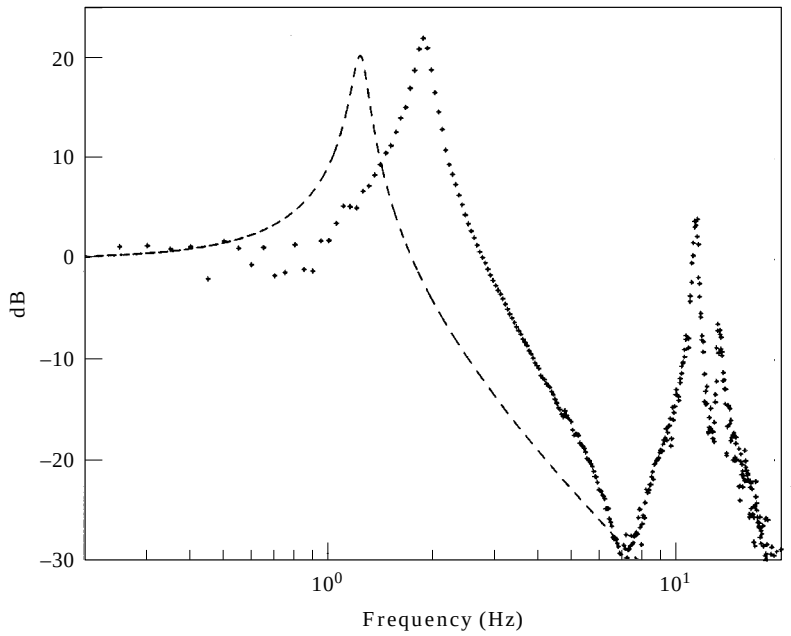

Figure 2. Transmissibility curves for dual-chamber configuration: – – –, original model; +, experimental data.

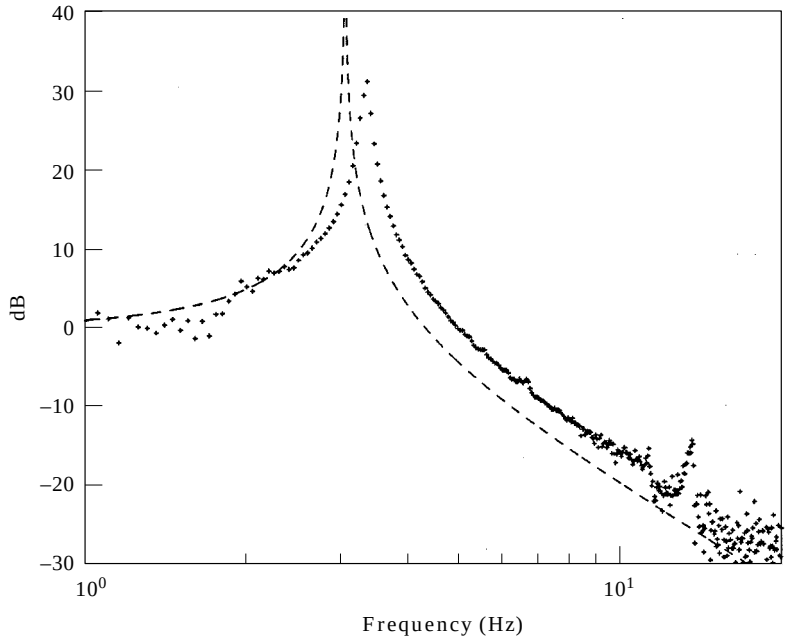

Figure 3. Transmissibility curves for single-chamber configuration: – – –, original model; +, experimental data.

The plots of the measured and the theoretical transmissibility for the single-chamber configuration, shown in Figure 3, also indicate a discrepancy. The theoretical model once again underestimates the resonant frequency. In addition, the measured data indicates the presence of damping in the system, whereas the theoretical model does not. A closer look at Figure 3 reveals that the difference between the theoretical and the experimental resonant frequencies is 9%. The theoretical resonant frequency is 3·05 Hz, while the experimental value is 3·35 Hz. Hence, compared to the case in the dual-chamber configuration, the existing models provide a better prediction of system behavior for single-chamber configuration. This fact will be exploited in the derivation of the improved model in section 4.

Based on the comparison between the measured and the theoretical transmissibility curves, we conclude that the existing theoretical isolator model provides a relatively poor prediction of the actual transmissibility. The term ''relatively poor'' should be qualified. In the context of closed loop system design, an accurate model is needed. Although this topic is not explored here in any depth, the issue of model uncertainty and closed-loop system performance is one of long-standing and active interest in the controls community. We anticipate the redesign of a pneumatic vibration isolator and the possible use of a notch filter tuned to the resonant frequency of the isolator. An accurate estimate of the resonant frequency and peak magnitude is essential for this application. Therefore, we will seek an improved isolator model that provides more accurate predictions of system performance. For other applications, the need may not be as clear, and

the requirement for a more accurate model should be examined on a case-by-case basis.

4. IMPROVED ISOLATOR MODEL

The transmissibility curves in Figures 2 and 3 indicate discrepancies between the predicted (modelled) and the measured performance of pneumatic vibration isolators. The modelled and measured transmissibility curves have roughly the same shape. However, the peak frequencies in the curves differ by up to 33%, and the peak magnitudes differ by up to infinity (for the undamped single chamber isolator). Furthermore, the predicted transmissibility magnitude is inaccurate at frequencies greater than the resonant frequency.

The relatively poor predictions provided by the theoretical model indicate a mismatch in the stiffness and damping characteristics. In the standard model, the dynamic response of a pneumatic vibration isolator depends upon the dimensions of the chambers, the piston area, the piston mass, and the dimensions of the flow restrictor. With the current apparatus, all of these parameters are known quite accurately. Thus, parametric uncertainty does not account for the difference between the predicted and the observed behavior. A faulty assumption of linearity could also be the cause of this difference. In our case, if the payload displacements are sufficiently large, the linearity assumption breaks down. However, as the payload displacements for base motion inputs are very small, the linearity assumption appears valid. The only remaining element that can be responsible for this mismatch is the diaphragm that supports the piston.

4.1. DIAPHRAGM MODEL

Previous models have assumed that the diaphragm does not affect the system performance. We see from the transmissibility curves, however, that such an assumption may be invalid. While it is difficult to model the effect of this diaphragm from first principles, it is possible to approximate it with the combination of a spring, dashpot, and hysteretic damper. When wrapped around the piston, the diaphragm forms a semi-torus. The observation that the available models predict experimental behavior better for the single-chamber configuration compared to the dual-chamber configuration (Figures 2 and 3) suggests that the diaphragm adds a certain stiffness, which is less significant in the stiff single-chamber configuration. This assertion is based on a 33% difference in resonant frequency for the dual-chamber configuration and a 10% difference for the single chamber configuration. The observation that the modelled and measured peak transmissibilities differed suggests that the diaphragm provides a damping mechanism. For the low displacement transmissibility tests, the addition of diaphragm viscous damping allows the modelled behavior to better approximate the measured behavior. During piston motion, the diaphragm bends and exhibits a rolling motion, which suggests a hysteretic damping (material damping) mechanism. Thus, hysteretic damping was also added to the model. We model the effect of the diaphragm by performing the following steps:

(1) approximate the dominant effects of the diaphragm with a viscous damper, a hysteretic damper, and a spring; (2) tune the values for each of these parameters using experimental data; (3) incorporate these effects in the model; (4) compare the predictions provided by the improved model with the observed behavior. The diaphragm model is illustrated in Figure 4, where it is characterized by the following parameters: c_d for viscous damping, h_d for hysteretic damping, and k_d for stiffness.

4.2. PARAMETER ESTIMATION

To estimate the diaphragm parameters in Figure 4, we systematically tuned the parameters to obtain a close fit between the measured and predicted responses. Once the parameters were tuned, we tested model performance against a set of data that was not used in tuning the parameters. This provided an independent means to validate the modified model. Two ranges of payload motion are used to estimate the diaphragm parameters:

Linear response range

The linear system response range involves small payload vibration amplitudes that generally occur for base motion inputs. The linear range is restricted to payload displacements smaller than 5 μm. In this range, the diaphragm parameters have constant values.

Non-linear response range

Non-linear system response occurs for large payload vibration amplitudes, which result from disturbance force inputs. For payload displacements greater than 5 μm, the diaphragm parameters are non-linear functions of vibration amplitude.

Low amplitude payload motion allows a linear model approximation to be used. Further, such motion allows three initial diaphragm parameters to be easily tuned. By *initial* we refer to the parameter values for small displacements. First, as the hysteretic energy loss for a single cycle of payload vibration depends on the square of the displacement [12–14], we can safely assume that this coefficient is negligible for small displacements. Second, we select a diaphragm stiffness k_d that makes the

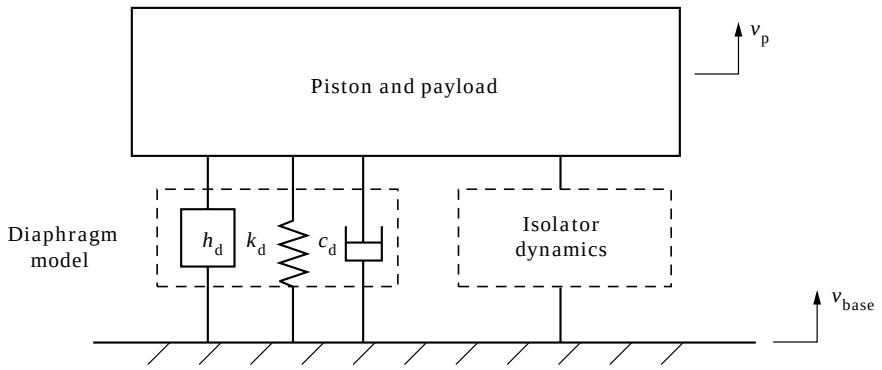

Figure 4. Mechanical model for pneumatic vibration isolator with the diaphragm.

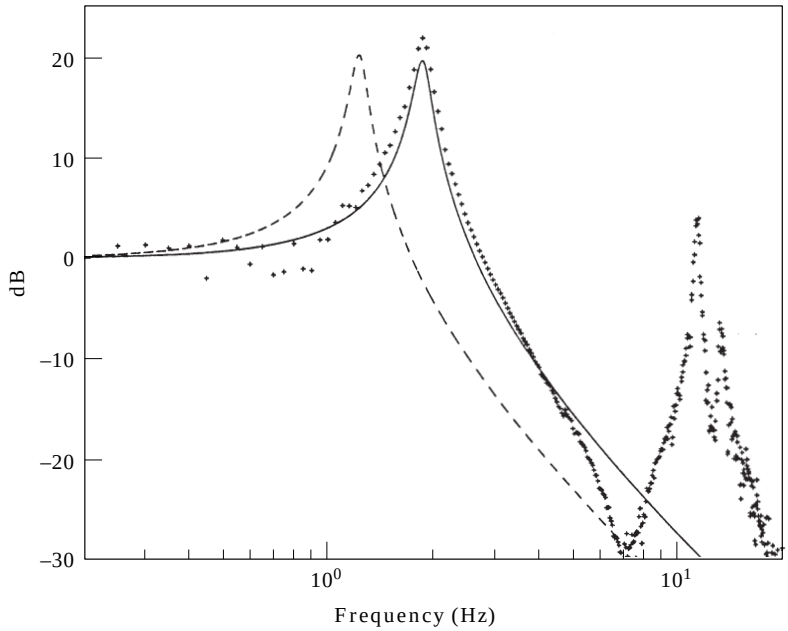

Figure 5. Transmissibility curves for dual-chamber configuration: ——, modified model; – – –, original model; +, experimental data.

peak frequencies in Figures 2 and 3 coincide; this value is 8170 N/m. Finally, we add viscous damping so that the magnitudes in these same two figures closely correspond; this damping value is 60 N·s/m. We see from the plots in Figures 5 and 6 that these initial values for the diaphragm parameters allow the model to provide a close approximation for transmissibility.

The initial diaphragm parameters provide an accurate prediction of transmissibility. However, if held constant, the same parameters provide relatively poor predictions of force disturbance response in the non-linear response range. Both the frequencies and the amplitudes of the theoretical and the measured responses differ. We conclude that the diaphragm parameters vary with large payload displacements.

The diaphragm appears to constitute the dominant non-linear mechanism in this isolator. Payload disturbance forces may produce large vibration amplitudes, causing the system to behave non-linearly. This non-linear behavior has three possible sources: gas compressibility, flow through the restrictor, or the diaphragm. Forces on the order of 1 kg produce payload displacements on the order of 1 mm. These displacements produce pressure differentials that are extremely small compared to the nominal pressures in the chambers. Therefore, the density of the gas in the chambers is essentially constant, implying that the non-linear behavior is not due to gas compressibility. A non-linearity in flow in the restrictor can originate from varying density or from the flow becoming turbulent. Since we have already ruled out a variation in density, only turbulent flow can be the source. Simulations show that the flow through the restrictor has

a Reynolds number less than 2000, implying laminar flow and linear behavior. This leaves only the diaphragm as the source of non-linear behavior in the system.

A qualitative understanding of the diaphragm behavior can be obtained from examining experimental data. Force disturbance response plots indicate that as the payload vibration amplitude increases, the natural frequency of the payload response and the amount of overshoot both decrease. This suggests that an increase in payload vibration amplitude is accompanied by (1) a decrease in the diaphragm stiffness, and (2) an increase in the diaphragm hysteretic damping. The exact functional dependencies of the stiffness and hysteretic damping coefficients on vibration amplitude are obtained using non-linear simulations with the Matlab Simulink package [15].

We tuned the displacement-dependent diaphragm stiffness and hysteretic damping parameters by matching measured and predicted force disturbance responses. This was performed for a range of loads. For the stiffness parameter, a step load was applied, eventually producing a constant displacement. A stiffness parameter value was chosen for this displacement, by trial and error, so that the period of the dynamic responses (measured and predicted) matched. This process was repeated for a range of loads and used to create a look-up table for stiffness versus displacement. Additional interpolation points were added to the table to obtain a smoother characterization of the diaphragm stiffness. A plot of this table is shown in Figure 7, where the softening effect of the diaphragm stiffness is evident. The hysteretic damping coefficient was chosen in a similar manner. For the same range of loads, this parameter was tuned so that the amplitude of the

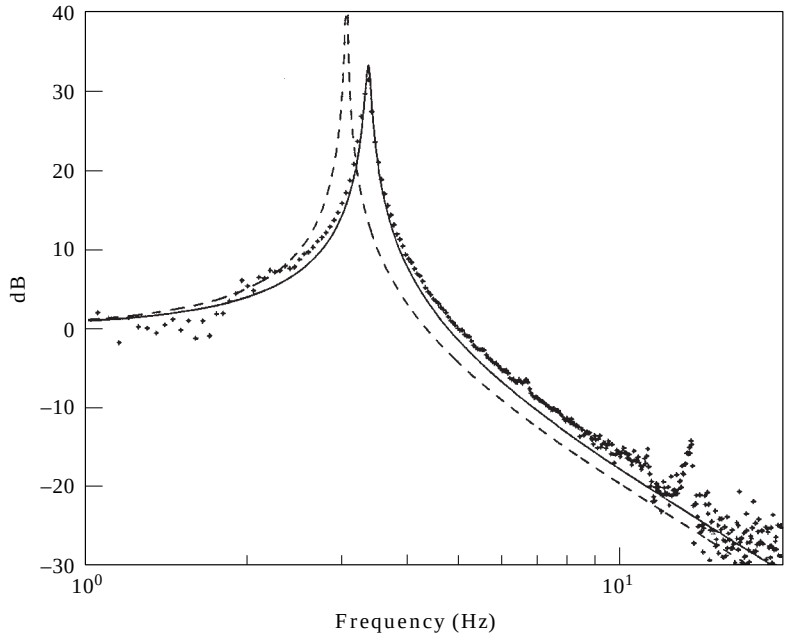

Figure 6. Transmissibility curves for single-chamber configuration: ——, modified model; – – –, original model; +, experimental data.

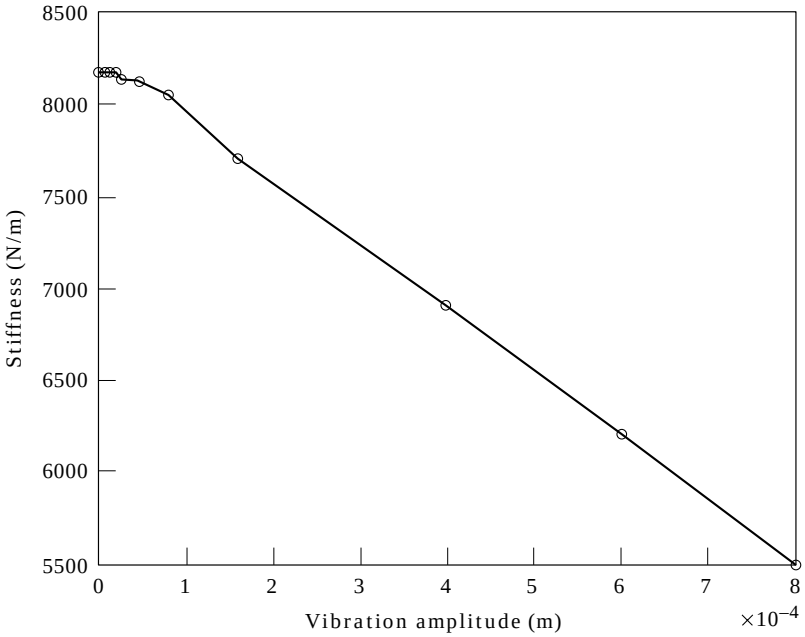

Figure 7. Stiffness characteristics of the diaphragm.

two dynamic responses matched. A plot of the associated look-up table is shown in Figure 8.

The improved isolator model incorporating this diaphragm model predicts system response accurately at all vibration amplitudes. Figure 9 represents

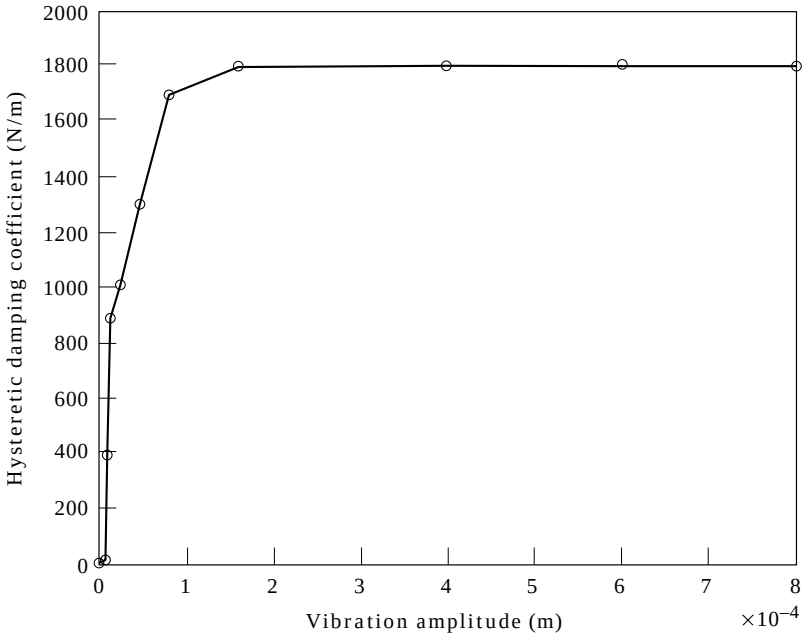

Figure 8. Hysteretic damping characteristics of the diaphragm.

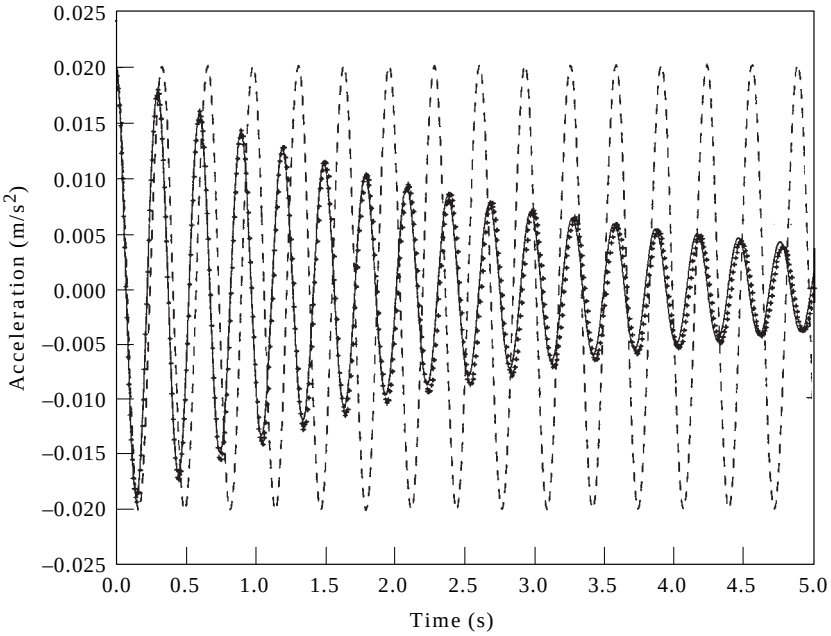

Figure 9. Force disturbance response of single-chamber configuration: ——, modified model; – – –, original model; +, experimental data.

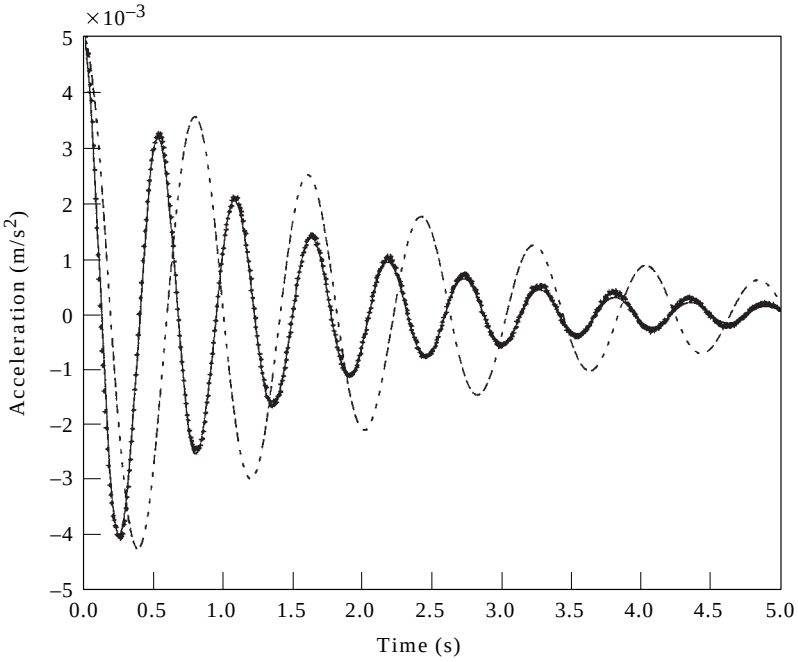

Figure 10. Force disturbance response of dual-chamber configuration: ——, modified model; – – –, original model; +, experimental data.

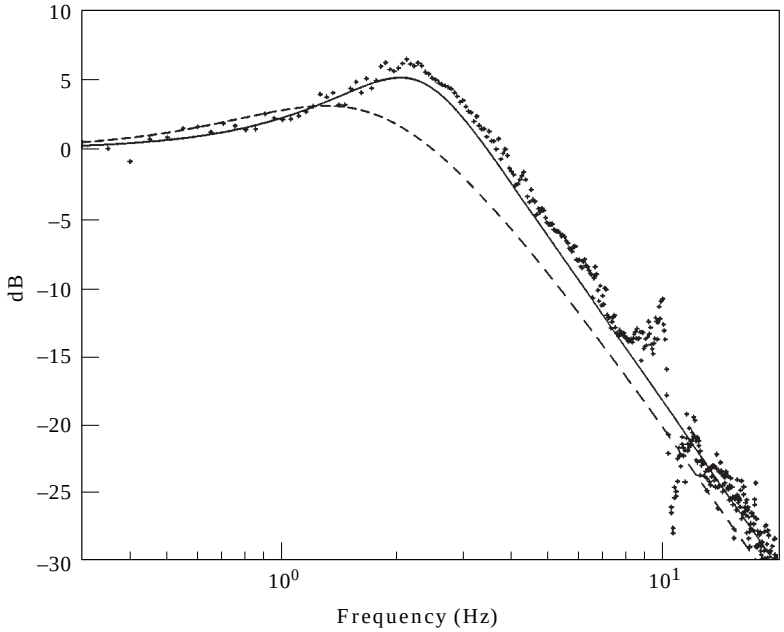

Figure 11. Transmissibility curves for new mount: ——, modified model; – – –, original model; +, experimental data.

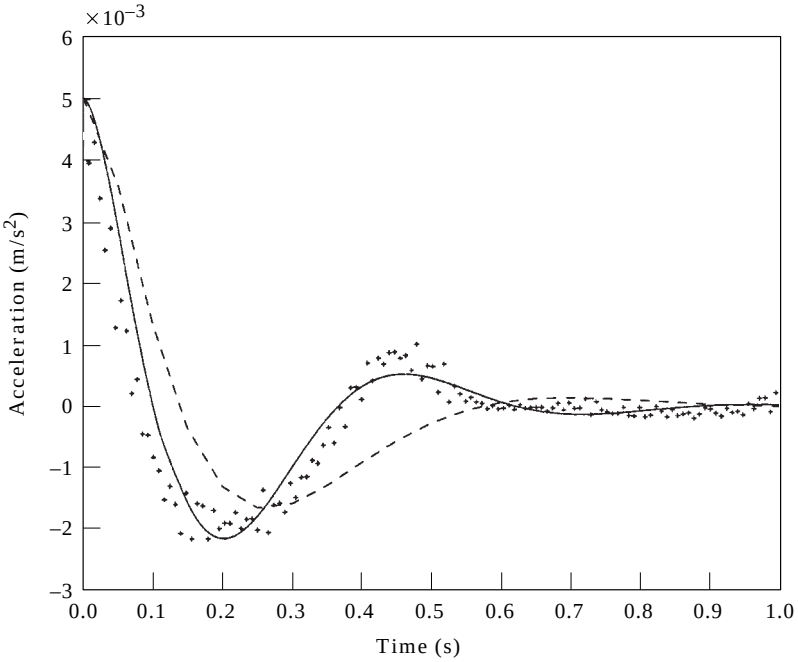

Figure 12. Force disturbance response of new mount: ——, modified model; – – –, original model; +, experimental data.

single-chamber system response for a disturbance force of 2·23 N. For this mount the improved model predicts actual response quite closely at all points. Figure 10 depicts the dual-chamber response for a disturbance force of 0·56 N. While the original model lags the experimental data and has higher maxima, the improved model again matches the experimental behavior perfectly. Hence, we conclude that the improved model predicts the experimental behavior accurately in the non-linear range, too.

4.3. VERIFICATION OF THE IMPROVED ISOLATOR MODEL

Thus far we have used the experimental data from two distinct mounts to derive an improved model of the pneumatic vibration isolator. We now check the applicability of the improved model to different mounts. Hence, we will employ a third mount, where the current flow restrictor is replaced with one that has a smaller diameter ($d = 0{\cdot}34$ mm), while the chamber sizes are kept constant. Figure 11 shows the transmissibility curves for the new mount. The resonant frequency of this mount is 2·05 Hz. The improved model incorporating the diaphragm mechanism predicts observed system response accurately, while the original model does not. Figure 12 shows the force disturbance response for the new mount for a disturbance force of 2·23 N. The improved model again predicts the actual response accurately and performs superior to the original model. The modified isolator model provides a much improved prediction of the dynamic response.

5. CONCLUSIONS

This analytical and experimental study of pneumatic vibration isolators makes a number of original contributions. First, we have used experimental data to show that the existing models of pneumatic vibration isolators provide an inaccurate prediction of actual system response. The discrepancy between measured and predicted responses originates from existing models neglecting a vital component of the system—the diaphragm. Second, we have proposed a model for the diaphragm that includes hysteretic damping, viscous damping, and stiffness elements. The proposed model was derived using transmissibility and force disturbance response curves, which displayed linear and non-linear system responses, respectively. Third, we analyzed the system non-linearities and identified the diaphragm to be the dominant non-linear element. Hence, the diaphragm model provided the linearity limits for the isolator. Fourth, we constructed an improved isolator model including the diaphragm model and the linear model of pneumatic vibration isolators. Finally, we showed that the improved model is successful in predicting both the frequency domain and the time domain responses for a different isolator configuration.

This paper provides several models for a pneumatic vibration isolator. Non-linear and linearized pneumatic chamber models are provided, as are non-linear and linearized models of the isolator diaphragm. These models serve as a reminder that different operating conditions often require different models.

Although not explored in this paper, the *relative importance* of the different components of the isolator models should also be evaluated before electing to include them in an overall model. For example, a very large payload (table) mass will decrease the natural frequency of an isolator and sharply attenuate the force disturbance response. In such a case, the chambers and diaphragm's effects on the table force disturbance response may be completely insignificant. Conversely, for a mass of 100 kg (or less), such as the one used in this paper, the chambers and the diaphragm have a very significant effect on system behavior, as discussed in section 4. For a linear analysis, a frequency domain model-order-deduction algorithm may provide some assistance in determining which components should be included in a system model [16].

The previous paragraph indicates that a large table mass diminishes the relative importance of the chambers and the diaphragm in the system model. A particular orifice diameter may have a similar effect. To reduce settling time, some design strategies suggest that the system damping be increased to provide critical damping. This increase is typically accomplished by decreasing the orifice diameter. (Note that a very small diameter will tend to reduce damping.) If the damping is increased in this manner, the effect of diaphragm damping on the system response may be less pronounced than that observed here, where the system is underdamped. Before adopting such a design strategy, however, it should be recognized that increased system damping will tend to degrade the high frequency transmissibility performance.

In conclusion, the improved isolator model developed in this paper provides a sound basis for developing an active control system using pneumatic vibration isolators. This work is in progress.

ACKNOWLEDGMENT

The authors wish to express their thanks to Kinetic Systems, Incorporated in Boston, MA, whose facilities were used to perform the experiments described in this paper.

REFERENCES

1. D. B. DeBra 1992 *CIRP Annals* **41**(2), 711–718. Vibration isolation of precision machine tools and instruments.
2. P. Burggraaf 1993 *Semiconductor International* December 42–46. Vibration control in the fab.
3. T. A. Cellucci and B. Houghton 1993 *Machine Design* November, 38–42. Vibration control without sticker shock.
4. D. B. DeBra 1984 *CIRP Annals* **33**(1), 351–356. Design of laminar flow restrictors for damping pneumatic vibration isolators.
5. H. V. Vu and B. J. Torby 1993 *American Society of Mechanical Engineers*, *Design Engineering Division* (*Publication*) *DE Vibration Isolation*, *Acoustics*, *and Damping in Mechanical Systems* **62**, 39–42. Pneumatic vibration isolation of a table traversed by a moving load.

6. J. L. Shearer 1954 *Ph.D thesis*, *MIT*, *Department of Mechanical Engineering*. Continuous control of motion with compressed air.
7. J. L. Shearer 1956 *Transactions of ASME* **78**, 233–242. Study of pneumatic processes in continuous control of motion with compressed air.
8. C. M. Harris and C. E. Crede 1961 *Shock and Vibration Handbook*. New York: McGraw-Hill.
9. B. W. Andersen 1967 *The Analysis and Design of Pneumatic Systems*. New York: Wiley.
10. R. C. Rosenberg and D. Karnopp 1983 *Introduction to Physical System Dynamics*. New York: McGraw-Hill.
11. D. Karnopp, D. Margolis and R. C. Rosenberg 1990 *System Dynamics*: *A Unified Approach*. New York: Wiley-Interscience.
12. S. S. Rao 1990 *Mechanical Vibrations*. New York: Addison-Wesley.
13. L. Meirovitch 1986 *Elements of Vibration Analysis*. New York: McGraw-Hill.
14. A. Nashif, D. Jones and H. Henderson 1985. *Vibration Damping*. New York: Wiley.
15. Matlab, Natick, MA. *Simulink Manual*, 1997.
16. B. H. Wilson and J. H. Taylor 1998 *Journal of Dynamics Systems*, *Measurement*, *and Control*. To appear. A frequency domain model-order-deduction algorithm for linear systems.

APPENDIX: NOMENCLATURE

c_d	diaphragm viscous damping coefficient, N · s/m
d	flow restrictor diameter, m
q	gravitational acceleration, m/s^2
h_d	diaphragm hysteretic damping coefficient, N/m
k_d	diaphragm stiffness, N/m
l	flow restrictor length, m
$\dot{m}_t$	mass flow rate of air into the top chamber, kg/s
$\dot{m}_b$	mass flow rate of air into the bottom chamber, kg/s
$\dot{m}_{tb}$	mass flow rate of air between top and bottom chambers, kg/s
m_p	payload mass, kg
n	polytropic exponent
v_{base}	base velocity, m/s
v_p	payload velocity, m/s
x_{base}	base displacement, m
x_p	payload displacement, m
A_p	effective piston area, m^2
C_p	specific heat of air at constant pressure, J · s/(N · K)
C_r	flow restriction constant, m^3/(Pa · s)
C_v	specific heat of air at constant volume, J · s/(N · K)
E	change in energy of air as a result of compression or expansion, J
F_d	disturbance force, N
H	total energy content of air, J
P_t	top chamber pressure, Pa
P_b	bottom chamber pressure, Pa
P_0	nominal pressure for top and bottom chambers, Pa
P_{atm}	atmospheric pressure, Pa
Q_t	volume flow rate of air through valve into the top chamber, m^3/s
Q_b	volume flow rate of air through valve into the bottom chamber, m^3/s
R	universal gas constant, J/(K.kg)
T	temperature, K
U	internal energy of air, J

V_b bottom chamber volume, m^3
V_t top chamber volume, m^3
V_{t_0} initial top chamber volume, m^3
W_t weight rate of flow of air into the top chamber, N/s
δP_t top chamber pressure differential, Pa
δP_b bottom chamber pressure differential, Pa
ρ gas density, kg/m^3
μ air viscosity, $Pa \cdot s$